

# The Coding of Temperature in the *Drosophila* Brain

Marco Gallio,<sup>1,2</sup> Tyler A. Ofstad,<sup>1,2,3</sup> Lindsey J. Macpherson,<sup>1,2</sup> Jing W. Wang,<sup>1</sup> and Charles S. Zuker<sup>1,2,3,\*</sup>

<sup>1</sup>Departments of Neurobiology and Neurosciences, University of California at San Diego, La Jolla, California 92093, USA

<sup>2</sup>Departments of Biochemistry and Molecular Biophysics and of Neuroscience, Howard Hughes Medical Institute, Columbia College of Physicians and Surgeons, Columbia University, New York, New York 10032, USA

<sup>3</sup>Janelia Farm Research Campus, Howard Hughes Medical Institute, Ashburn, Virginia 20147, USA

\*Correspondence: cz2195@columbia.edu

DOI 10.1016/j.cell.2011.01.028

## SUMMARY

Thermosensation is an indispensable sensory modality. Here, we study temperature coding in *Drosophila*, and show that temperature is represented by a spatial map of activity in the brain. First, we identify TRP channels that function in the fly antenna to mediate the detection of cold stimuli. Next, we identify the hot-sensing neurons and show that hot and cold antennal receptors project onto distinct, but adjacent glomeruli in the Proximal-Antennal-Protocerebrum (PAP) forming a thermotopic map in the brain. We use two-photon imaging to reveal the functional segregation of hot and cold responses in the PAP, and show that silencing the hot- or cold-sensing neurons produces animals with distinct and discrete deficits in their behavioral responses to thermal stimuli. Together, these results demonstrate that dedicated populations of cells orchestrate behavioral responses to different temperature stimuli, and reveal a labeled-line logic for the coding of temperature information in the brain.

## INTRODUCTION

The role of our senses is to create an internal representation of the physical and chemical features of the external world. Sight, hearing, touch, smell, and taste define the basic palette used by scientists, artists, writers, and poets to illustrate how we capture the world in our brains (Shakespeare went even further, and in his Sonnet 141 tells us about the struggles between the senses and the heart). Of course, we now recognize several additional sensory systems, most prominently perhaps temperature sensing.

Recent advances in the study of mammalian thermosensation have provided fundamental insight into molecular mechanisms mediating hot and cold temperature detection (Jordt et al., 2003; McKemy, 2007; Patapoutian et al., 2003). The detection of thermal stimuli relies on receptor proteins activated directly by changes in temperature. At present, four mammalian heat-activated (TRPV1-4) and two cold-activated (TRPM8 and TRPA1)

ion channels, all members of the Transient Receptor Potential (TRP) family, have been shown to function as temperature receptors. Some of these thermosensors operate in the noxious (TRPV1, TRPV2, and TRPA1), and some in the innocuous (TRPV3, TRPV4, TRPM8) temperature range (Basbaum et al., 2009; Caterina et al., 2000, 1999, 1997; Colburn et al., 2007; Dhaka et al., 2007; Guler et al., 2002; Jordt et al., 2003; Lee et al., 2005; McKemy et al., 2002; Moqrich et al., 2005; Peier et al., 2002a, 2002b; Smith et al., 2002; Story et al., 2003; Xu et al., 2002).

Several cell types are likely to function as peripheral temperature sensors in mammals. Most notably, neurons located in the dorsal root ganglion (DRG) project to the skin, where they detect changes in temperature both in the noxious and innocuous range (Basbaum et al., 2009; Jordt et al., 2003; Patapoutian et al., 2003). TRP channel expression defines at least four DRG neuron sub-classes: TRPV1 expressing (hot nociceptors), TRPV1+TRPA1 expressing (putative hot-cold polymodal nociceptors), TRPM8 expressing (cold sensors), and TRPV2 expressing cells (very high threshold hot nociceptors) (Basbaum et al., 2009; Jordt et al., 2003; McKemy, 2007; Patapoutian et al., 2003). Surprisingly, the “warm receptors” TRPV3 and TRPV4 do not appear to be expressed in DRG neurons, but rather in keratinocytes within the skin (TRPV3; (Peier et al., 2002b), or very broadly in both neural and non-neural tissues (TRPV4; (Plant and Strotmann, 2007). The in vivo requirement of TRPs as thermosensors was substantiated by the characterization of knock-out mice lacking TRPV1, TRPV3, TRPV4 or TRPM8 (Caterina et al., 2000; Colburn et al., 2007; Dhaka et al., 2007; Lee et al., 2005; McKemy, 2007; Moqrich et al., 2005). Interestingly, while the phenotypes were often partial and compound supporting a model involving multiple (possibly overlapping) receptors (Lumpkin and Caterina, 2007), some cases were very clear suggesting a 1:1 correspondence between receptor expression and behavior. For example, TRPM8 mutant mice are dramatically impaired in their behavioral and physiological responses to cold temperatures (Bautista et al., 2007; Colburn et al., 2007; Dhaka et al., 2007). As TRPM8 is expressed in most, if not all, cold-sensing neurons (Dhaka et al., 2008; Kobayashi et al., 2005; Takashima et al., 2007) but not in hot nociceptors (Kobayashi et al., 2005), these results suggest that the coding of temperature may be orchestrated by the activity of dedicated cell types, each tuned to respond to a defined temperature range (Lumpkin and Caterina, 2007).

How do animals represent and process thermal stimuli? *Drosophila* provides an attractive system to study temperature coding: flies possess sensory systems anatomically and genetically simpler than those of vertebrates, and critically depend on quick, reliable and robust temperature sensing for survival (an important adaptation of poikilothermic organisms). In *Drosophila*, two related TRP channels have been proposed as temperature receptors: *painless* (Sokabe et al., 2008; Tracey et al., 2003) and *dTRPA1* (Hamada et al., 2008; Kwon et al., 2008; Rosenzweig et al., 2005). The *painless* channel is activated by high, “noxious” heat (>42–45°C; (Sokabe et al., 2008), and is expressed in peripheral multi-dendritic neurons of the larval body wall (Tracey et al., 2003). As *painless* mutants also fail to react to mechanical injury (Tracey et al., 2003), this channel appears to be required for the function of bimodal thermal/mechanical nociceptors. *dTRPA1* was originally described as a candidate hot receptor based on its ability to respond to warm temperatures in heterologous expression systems (Viswanath et al., 2003). Surprisingly, *dTRPA1* doesn’t function in the PNS, but rather in a small cluster of neurons within the brain (Hamada et al., 2008). In addition to internal thermosensors, adult flies have been suggested to have temperature receptors located in antennae (Sayeed and Benzer, 1996; Zars, 2001).

To begin studying temperature coding in *Drosophila*, we isolated mutants affecting behavioral responses to temperature. Here, we describe candidate cold temperature receptors in *Drosophila* and identify the peripheral neurons and the thermosensory organs in which they function. We also used live imaging to record the activity of the peripheral hot and cold thermosensors and studied their function and projections to the brain. Our results substantiate a labeled line wiring logic for cold and hot sensors, and illustrate how the activity of these dedicated cells may be used to orchestrate an animal’s temperature preference.

## RESULTS

### **brivido Genes Are Necessary for Behavioral Responses to Cold Temperatures in *Drosophila***

In order to identify potential cold receptors in *Drosophila*, we screened a collection of candidate *P* element insertions for altered temperature preference in a simple two-choice assay. Fifteen flies from each *P* element line were allowed to distribute in a small arena divided into 4 quadrants, two were set to a reference temperature (25°C), and two to a test temperature (ranging from 11 to 39°C). The time spent by the flies in each quadrant (in a 3 min trial) was then computed to calculate an avoidance index for the test temperature (see [Experimental Procedures](#) for details). Wild-type flies display a clear preference for temperatures in the range of 24°C–27°C (Sayeed and Benzer, 1996), with robust avoidance to colder and warmer temperatures (Figure 1). One of the candidate lines, however, exhibited a markedly altered behavior, with a clear deficit in their aversion to cold temperatures (NP4486; Figure S1, available online). Interestingly, this line carries a *P* element insertion approximately 2 Kb downstream of a predicted Transient Receptor Potential (TRP) ion channel (CG9472; Figure 1). To determine whether this ion channel is in fact involved in thermosensation, we screened for

classical loss-of-function mutations within the CG9472 coding region by Tilling (McCallum et al., 2000), and recovered a non-sense mutation (*brv1*<sup>L563 > STOP</sup>) that truncates the protein within the highly conserved ion transporter domain (Figure 1; (Bateman et al., 2000). *brv1*<sup>L563 > STOP</sup> homozygous mutants are viable and display no obvious morphological defects. However, these mutant flies, much like the original NP4486 *P* element insertion line, exhibit a selective deficit in their avoidance to cold temperatures (Figure 1). Because of this potential cold temperature sensing deficit, we named CG9472 *brivido-1* (*brv1*, Italian for shiver).

*Brv1* is a member of the TRPP (polycystin) subfamily of TRP ion channels (Montell et al., 2002). The *Drosophila* genome encodes two additional uncharacterized TRPPs, CG16793 and CG13762 (here named *brivido-2* and *-3*; Figure 1). Thus, we set out to test if one or both of these TRP genes might be important for thermosensation. Using Tilling, we screened for potential loss of function mutations in *brv2*, and recovered several mutants, including one that carries a non-sense mutation that truncates the protein before the ion transporter domain (*brv2*<sup>W205 > STOP</sup>). Figure 1 shows that *brv2* mutants display dramatic deficits in their avoidance to cold temperatures, even as low as 11°C. Importantly, this defect is due to the loss of the *brv2* TRP channel, as introduction of a wild-type gene completely restores normal temperature preference to the mutant flies (Figure S1). *brv3* maps to the X chromosome, and was therefore not amenable to Tilling using the existing mutant collections (Koundakjian et al., 2004). Hence, we targeted an inducible *brv3* RNAi transgene (Ni et al., 2009) to all neurons (under the control of the *scratch* promoter, strongly expressed in the PNS; (Roark et al., 1995) and monitored the resulting flies for temperature choice defects. As seen for *brv1* and *brv2* mutants, reducing *brv3* transcript levels (Figure 1 and Figure S1, and see below) also impacted the animal’s specific aversion to cold temperatures. Together, these results reveal an important role for the Brivido TRP ion channels in cold temperature sensing, and led us to hypothesize that Brv-expressing cells might function as cold thermosensors in *Drosophila*.

### **brv1 Expression Defines a Population of Antennal Cold Receptors**

Little is known about the identity or location of the cells that act as cold temperature receptors in *Drosophila*. Electrophysiological studies in other insects, however, have singled out the antenna as an important substrate for cold detection (Altner and Loftus, 1985). The original *brv1* *P* element insertion line also functions as an enhancer trap (Hayashi et al., 2002), therefore we used these flies to examine potential sites of *brv1* expression in the antenna. NP4486-Gal4 drives UAS-GFP reporter expression in different sets of cells in the antenna: (a) mechanosensory neurons of the 2nd antennal segment (Figure S2), (b) three ciliated neurons at the base of the arista (Figure 2, open arrowheads), and (c) a small number (~15–20) of neurons in the sacculus region of the 3rd antennal segment (Figure 2, arrowhead). The expression in all 3 sites reflects the expression of the native *brv1* gene as all are labeled in *in situ* hybridization experiments with an antisense *brv1* probe (Figure S2). Could any of these neurons be the elusive antennal

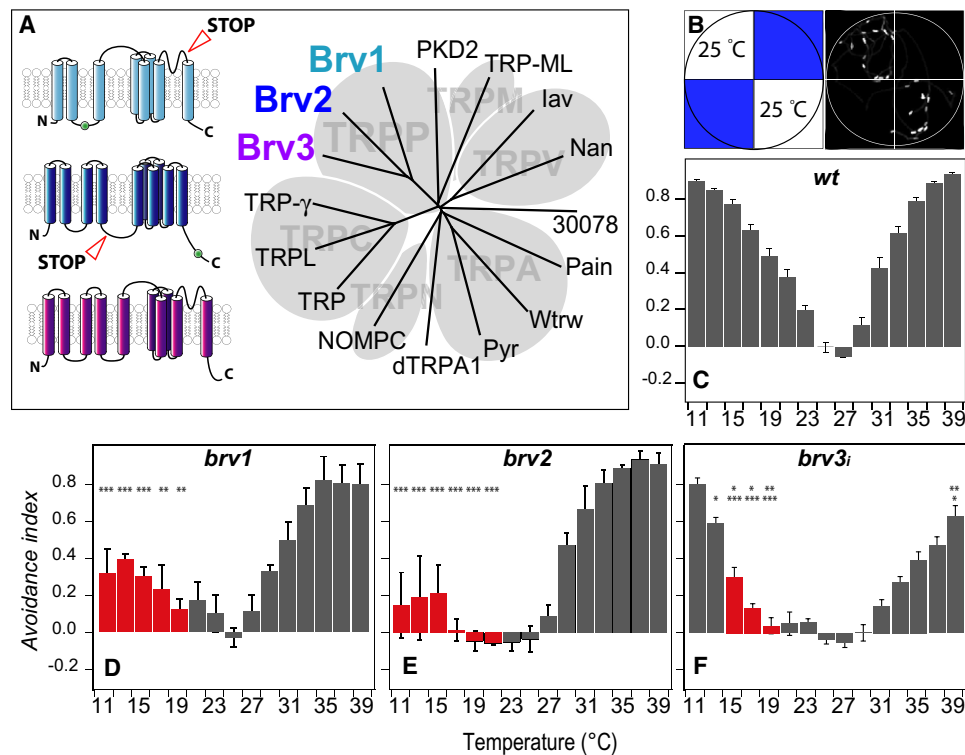


**Figure 1. Temperature Preference Phenotypes of *brivido* Mutants**

(A) Dendrogram tree of TRP channels in *Drosophila*; *brivido* genes encode three members belonging to the TRPP subfamily (Montell et al., 2002). The diagrams to the left illustrate the proposed secondary structure of Brv proteins, and the location of loss-of-function mutations in *brv1* and *brv2* (STOP).

(B and C) Two-choice assay of temperature preference in control flies. (B) Groups of 15 flies are tested in a chamber whose floor is tiled by four independently controlled peltier elements. In each trial, a new test temperature (represented in blue) is chosen, and the position of the flies recorded for 180 s. Set and reference temperatures are then switched for an additional 3 min trial. (C) Cumulative images of the flies' position throughout the trial (illustrated in the right of panel b) are analyzed to compute an avoidance index for each test temperature (gray bars in c, test temperatures varied between 11°C and 39°C, Reference temperature = 25°C; n = 10, mean ± SEM).

(D–F) Temperature preference phenotypes of (D) *brv1*<sup>L563 > STOP</sup>, (E) *brv2*<sup>W205 > STOP</sup>, and (F) *scratch-Gal4 > brv3*(RNAi) flies (n > 5, mean ± SEM). Red bars denote AI values significantly different from controls in the cold range (p < 0.05). In (F), lower asterisks indicate significant difference from *scratch-Gal4/+* (Figure S1D) and upper asterisks from *+/UAS-brv3*<sup>RNAi</sup> (Figure S1E). In all panels, \*\*\* = p < 0.001, \*\* = p < 0.01, \* = p < 0.05, ANOVA. See also Figures S1F–S1H.

cold receptors? To answer this question, we expressed G-CaMP, a genetically-encoded calcium activity indicator (Nakai et al., 2001; Wang et al., 2003), under the control of NP4486-Gal4 and investigated the functional responses of the *brv1*-expressing antennal neurons to temperature stimulation. To ensure the integrity of the tissue during functional imaging, we used a set up that permits monitoring G-CaMP's fluorescence in real time through the cuticle, yet still maintains single-cell resolution (see Experimental Procedures). Our results (Figure 2 and Figure S2) demonstrate that *brv1*-expressing neurons, both in the arista and in the sacculus (but not in the 2nd antennal segment, data not shown) respond rapidly, robustly, and selectively to cooling stimuli. Remarkably, these cells are activated by temperature drops as small as ~0.5°C, and their responses reliably mirror the kinetics and amplitude of the stimulating cold pulse (Figure 2). Importantly, these cells are not activated by hot stimuli (see below).

Do Brvs function together in thermosensation? We have attempted to define the cellular sites of expression for each of the 3 *brv* genes, but have been unable to map the sites of expres-

sion for *brv2* and *brv3* (data not shown). However, three pieces of evidence strongly argue that *brvs* are co-expressed in cold sensing neurons. First, loss-of-function of any one of the *brv* genes results in strikingly similar defects in the behavioral responses of adult flies to cold stimuli (Figure 1). Second, targeting *brv3* RNAi to *brv1*-expressing neurons (under the control of NP4486-Gal4) results in a cold sensing deficit comparable to ubiquitous *brv3* RNAi expression (Figure S1H). Third, we imaged cold-induced calcium transients in *brv1* and *brv2* mutant animals. Our results (Figure 2) show that the cold-evoked responses of *brv1*-expressing cells are severely affected in either *brv1* or *brv2* mutant backgrounds. These results demonstrate that *brvs* are required in the same neurons, and further substantiate *brv*-expressing cells in the antenna as cold temperature receptors.

#### A Population of "Hot" Receptors

In addition to the three *brv1*-expressing cold-sensing cells, the arista also houses three additional neurons, for a total of six in each arista (Foelix et al., 1989). We reasoned that an ideal

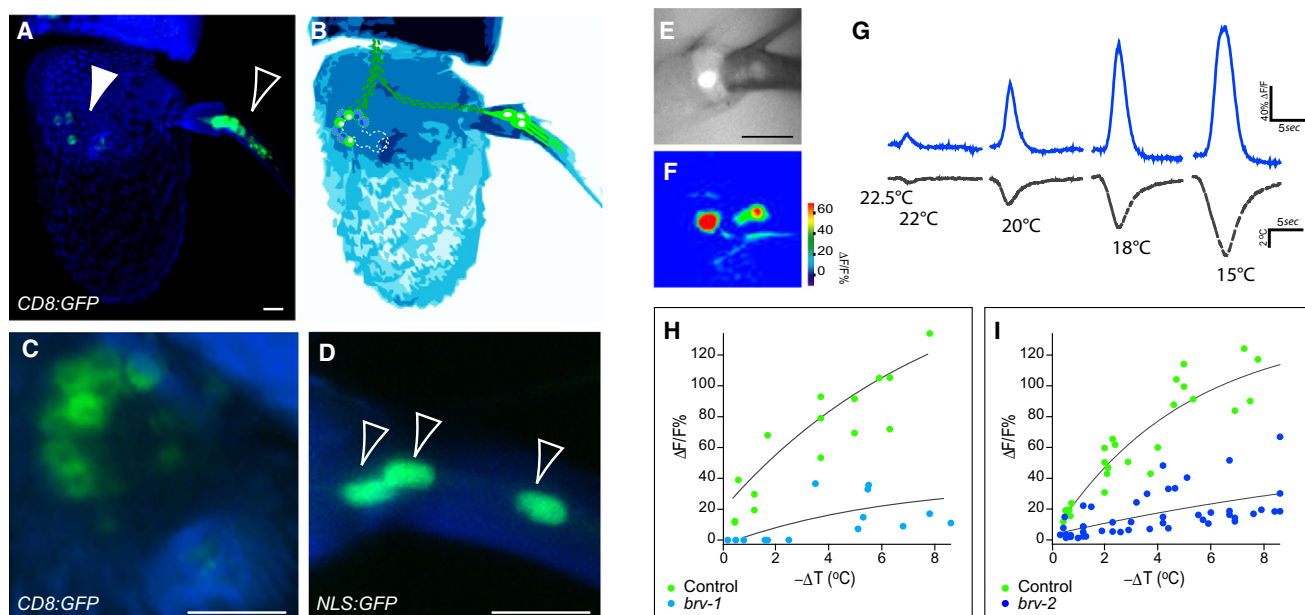


**Figure 2. *brv1* and *-2* Function in Cold Temperature Reception In Vivo**

(A–D) Cold sensing neurons in the *Drosophila* antenna are revealed by expression of fluorescent reporters under the control of the *brv1* enhancer trap NP4486-Gal4. (A) NP4486-Gal4 drives CD8:GFP expression in neurons located in the sacculus region (arrowhead), and in a small number of neurons at the base of the arista (open arrowhead). (B) *Camera lucida*-style drawing representing the position of the *brv1*-expressing neurons (the sacculus is represented by a dashed line drawing). (C) High-magnification confocal stack showing ~15–20 *brv1*-expressing neurons in the sacculus. (D) An NLS:GFP nuclear localized reporter marks the 3 *brv1*-expressing cells in the arista (open arrowheads).

(E and F) *brv1*-expressing arista neurons respond to cooling stimuli. Shown in (E) is a basal fluorescence image, and (F) the maximal response during a stimulus of  $\Delta t \sim 5^\circ\text{C}$  (from  $22^\circ\text{C}$  to  $17^\circ\text{C}$ ), the lookup table represents  $\Delta F/F\%$ . (G) Temperature responses are reversible and scale with the magnitude of the stimulus (responses of a single cell are shown as blue traces,  $\Delta F/F\%$ ; gray traces denote stimuli in  $^\circ\text{C}$ ; in all panels the scale bar represents  $10\ \mu\text{m}$ ).

(H and I) Loss-of-function mutations in *brivido 1* and *-2* severely affect the responses of the arista cold-sensing neurons to cooling. Shown are G-CaMP responses from (H) *brv1*<sup>L563 > STOP</sup> (light blue dots,  $n = 5$ ) and (I) *brv2*<sup>W205 > STOP</sup> (dark blue dots,  $n = 10$ ) mutant flies compared to control flies (green dots); G-CaMP was expressed under the pan-neural driver *elav*-Gal4. Each dot represents the response of a single cell to a stimulus; each animal was subjected to a maximum of 5 stimuli of different intensity (see *Experimental Procedures*,  $n = 5$  animals in [H] and  $n = 10$  in [I]). Note the significant reduction in the responses of mutant animals; we suggest that the small, residual activity seen in each of the mutant's lines is likely the result of overlapping function among the different *brv* genes (see also *Figure S2*).

temperature sensing-organ should house cold- and hot-sensors, and therefore examined whether these three extra neurons may function as hot temperature receptors. To sample the activity of the six neurons in the same preparation, we engineered flies expressing G-CaMP in all arista neurons under the control of the pan-neural driver *elav*-Gal4 (Lin and Goodman, 1994), and monitored their responses to cold- and hot temperature stimuli. All six arista neurons indeed responded selectively to temperature changes: 3 neurons exhibited calcium increases to warming, but not cooling, and 3 to cooling but not warming stimuli (Figure 3). Much like the *brv*-expressing cold receptor neurons, arista hot-sensing neurons were activated by temperature increases as small as  $\sim 0.5^\circ\text{C}$ , and their responses closely tracked the temperature stimulus (Figure S3). Interestingly, each population was inhibited by the opposite thermal stimuli, with hot cells displaying a decrease in  $[\text{Ca}^{2+}]_i$  in response to cold stimuli, while the cold cells exhibit a decrease in  $[\text{Ca}^{2+}]_i$  in response to hot stimuli (Figure 3). Hence, the antenna contains two distinct sets of thermoreceptors that together operate as opposite cellular sensors: one set of cells that is activated by a rapid rise in temperature but is inhibited by cold stimuli, and another

that is activated by cold temperature but is inhibited by hot stimuli (Figure 3).

Recently, another TRP ion channel, *dTRPA1*, has been proposed to function as a warmth receptor in a small group of neurons in the *Drosophila* brain (i.e., an internal brain thermosensor; (Hamada et al., 2008). Thus, we examined whether *dTRPA1* plays a role in the responses of the antennal hot sensing cells by recording the thermal-induced activity of these neurons in a *dTRPA1* mutant background. Our results demonstrated no significant differences in hot responses between wild-type and mutant animals (Figure S3), thus ruling out a significant role for *dTRPA1* in the detection of hot temperature by the antenna.

### Distinct Brain Targets for Hot and Cold Thermoreceptors

How is the antennal temperature code relayed to the brain? Do hot and cold channels converge onto the same target, or do they project to different brain regions? To address these questions, we tracked the projections of the antennal thermoreceptors to the brain. To follow the projections of the cold receptors,



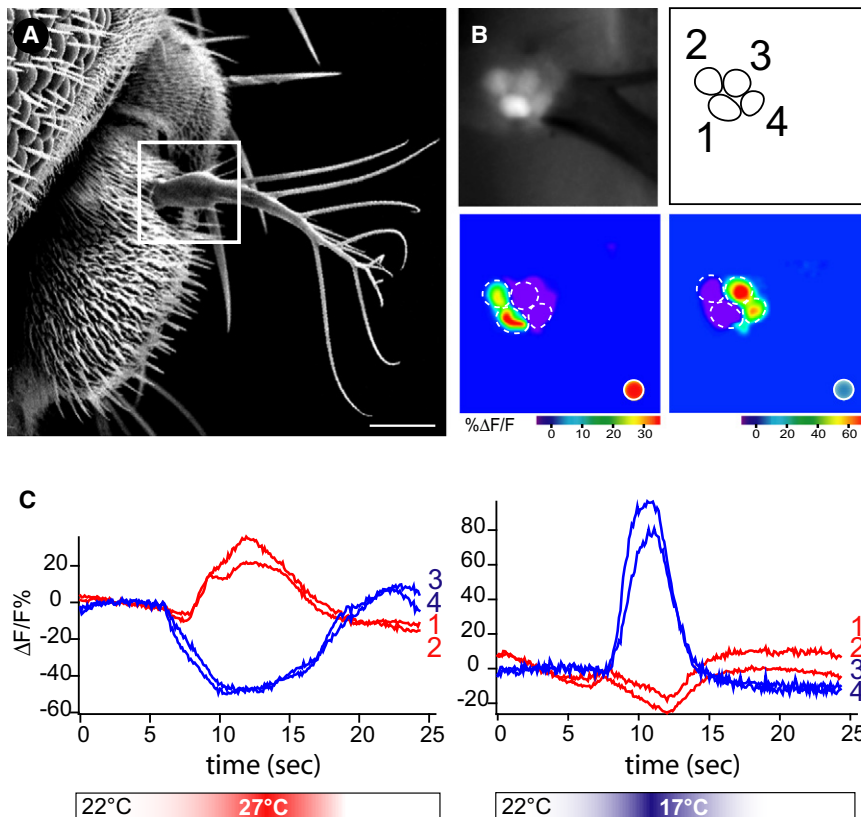


**Figure 3. Hot and Cold temperature Receptors in the *Drosophila* Antenna**

(A) Scanning electron micrograph of the *Drosophila* antenna. The arista (white box) houses six neurons, four of which are visible on the focal plane shown in (B).

(B) Basal fluorescence and maximal response images of 4 neurons expressing G-CaMP under the control of *elav-Gal4*. Functional imaging reveals that these cells respond to either hot (cells 1 and 2) or cold (cells 3 and 4) thermal stimuli (Stimuli are  $\Delta t \sim 5^\circ\text{C}$  from  $22^\circ\text{C}$ ; red dot: hot stimulus; blue dot: cold stimulus).

(C) Response profile of the two hot- (cells 1 and 2 in panel [B]) and the two cold-sensing neurons (cells 3 and 4 in panel [B]) to a stimulus of  $\Delta t \sim 5^\circ\text{C}$ ; red traces denote responses of hot cells, and blue traces depict the cold cells. Note that cold sensing neurons display a drop in intracellular calcium in response to hot stimuli, and the hot-sensing neurons display a decrease in intracellular calcium in response to warming (scale bar represents  $20 \mu\text{m}$ , see also Figure S3).

we expressed a membrane targeted GFP (CD8:GFP) under the control of the *bv1* enhancer trap, NP4486-Gal4. Because NP4486 is also expressed in the brain (Figure S2), we relied on an intersectional strategy to restrict expression of NP4486-Gal4 only to antennal neurons (e.g., using *eyeless-flippase* expressed in the antenna but not in the brain, and a  $\text{FRT} > \text{Gal80} > \text{FRT}$  transgene; see [Experimental Procedures](#) for details). Figure 4 shows that projections from *bv1* expressing cold-sensing neurons converged onto a previously uncharacterized region of the fly brain, arborizing into a discrete glomerulus lying at the lateral margin of the Proximal Antennal Protocerebrum (PAP).

What about the hot receptors? In order to track the projections of the “hot” aristal neurons, we had to first identify selective drivers for these cells. We screened Gal4 lines for reporter expression in the arista and tested candidate lines on two criteria. On the one hand, positive lines had to drive expression of a GFP reporter in only 3 of the 6 arista cells. On the other hand, these labeled cells should respond to hot but not cold stimuli. Indeed, one line, HC-Gal4, drove CD8:GFP expression in 3 out of the 6 aristal thermoreceptors, but not in any other cell in the antenna or CNS. In addition, G-CaMP functional imaging experiments proved that these 3 neurons respond specifically to warming, but not cooling stimuli (Figure S3). Therefore, using HC-Gal4 and CD8:GFP we examined the projections of the hot receptors. Figure 4 demonstrates that hot receptors also target the PAP. Notably, these projections

are clearly segregated from those originating in the cold-sensing neurons, converging to a glomerulus that is just adjacent, but not overlapping the one targeted by cold cells (Figure 4). Strikingly, the previously described internal “warm” receptors (expressing dTRPA1; [Hamada et al., 2008](#)) also send projections to the hot glomerulus (Figure S4). Taken together, these results reveal a thermotopic map of projections in the PAP.

### A Functional Map of Temperature Representation in the Protocerebrum

We reasoned that the topographic map of hot- and cold projections in the PAP would translate into a functional representation of temperature in the brain. Thus, we used two-photon calcium imaging ([Denk et al., 1990](#)) to examine activity in the brains of flies expressing G-CaMP under the control of either NP4486-Gal4 or HC-Gal4. Indeed, the PAP glomerulus targeted by the cold neuron projections displayed robust calcium transients in response to cold stimuli, while the PAP glomerulus formed by the projections from the hot neurons was selectively stimulated by hot temperature (Figure 5). Importantly, the activity of cold and hot glomeruli was proportional to the stimulus intensity (Figure 5 and Figure S5) and -as seen in the cell bodies- each glomerulus also responded to the opposite temperature stimulus with a decrease in  $[\text{Ca}^{2+}]_i$ . We also expressed G-CaMP pan-neurally (under the control of *elav-Gal4*) so as to simultaneously image both PAP glomeruli, and examined the responses to hot and cold stimulation. Again, only the two PAP glomeruli responded to thermal stimulation, and displayed a high degree of sensitivity and selectivity: the “hot” glomerulus was activated exclusively by warming, and the “cold” one by cooling stimuli (Figure 5). Finally, to validate the antennal thermosensors as the major drivers of PAP activity, we showed that surgical

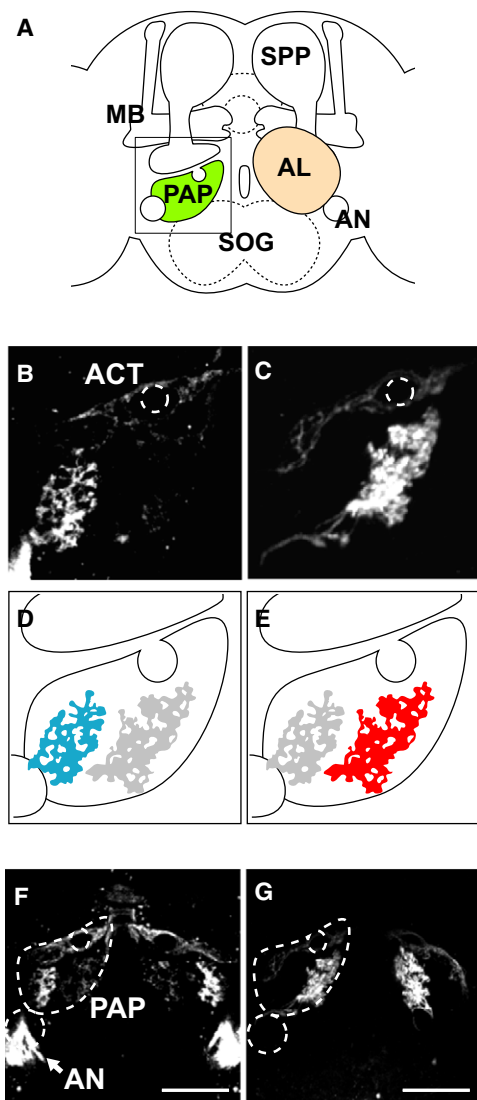


**Figure 4. Hot and Cold Fibers Define Two Distinct Glomeruli in the Protocerebrum**

(A–G) Hot and cold antennal neurons target two distinct, but adjacent glomeruli in the proximal antennal protocerebrum (PAP). (A) Schematic representation of major centers in the fly brain highlighting the position of the PAP (in green). The PAP lies just below the antennal lobe (AL, not shown on the left side of the brain to reveal the PAP); MB, mushroom bodies. SPP: super peduncular protocerebrum. AN: antennal nerve. SOG: sub esophageal ganglion. (B) PAP projections of antennal cold receptors. NP4486-Gal4 flies carrying ey-FLP (active in the antenna) and a tubulin-FRT > Gal80 > FRT transgene, reveal the projections of cold thermoreceptors to the PAP (see text and [Experimental Procedures](#) for details). Cold receptor afferents coalesce into a distinct glomerulus at the lateral margin of the PAP (ACT, antennocerebral tract). (C) Hot receptors (labeled by CD8:GFP driven by HC-Gal4) also target the PAP, forming a similar, but non overlapping glomerulus. (D and E) Schematic illustration of the PAP, with superimposed tracings of the projections shown in panels (B) and (C) (blue: cold receptors; red: hot receptors). (F and G) Low magnification confocal stacks showing symmetrical innervation of the PAP. Panel (F) shows a brain from a NP4486-Gal4 fly and panel (G) from a HC-Gal4 animal. The strong labeling seen in the antennal nerve (AN) of NP4486-Gal4 flies originates in the NP4486-expressing mechanoreceptors of the second antennal segment; these target the Antennal and Mechanosensory Motor

resection of a single antennal nerve dramatically reduced PAP responses on the side of the lesion, while bilateral resection affected responses on both sides of the brain ([Figure S5](#) and data not shown). Together, these results validate a functional temperature map in the brain, and demonstrate that hot and cold stimuli are each represented by a unique spatial pattern of activity in the proximal antennal protocerebrum.

### Labeled Lines for Temperature Processing in *Drosophila*

To address how the segregated cold and hot inputs into the PAP might be used to produce temperature choice behavior, we examined the impact of functionally inactivating either the hot- or the cold-sensing neurons by transgenically targeting expression of tetanus toxin light chain to these cells (TeNT is an endopeptidase that removes an essential component of the synaptic machinery, [Sweeney et al., 1995](#)). We hypothesized that if a comparison of both inputs (responding to hot and cold) is always necessary to determine the fly's preferred temperature, then inactivating either cell type should result in a deficit across temperatures. However, if the hot and cold inputs operate as independent conduits, then altering one input may not affect the animal's behavioral responses to the opposite temperature. To inactivate the cold antennal thermoreceptors, we expressed TeNT under the control of NP4486, again utilizing an ey-FLP based intersectional strategy to minimize toxin expression in other brain circuits (see [Experimental Procedures](#) for details); to abolish synaptic activity from the hot cells we expressed TeNT under HC-Gal4. Our results ([Figure 6](#)) demonstrate that silencing either the hot- or the cold-sensing neurons results in a highly selective loss of temperature behavior, with cold-cell inactivation affecting only cold-avoidance, and hot-cell inactivation impacting only behavioral aversion to hot temperatures. Thus, the anatomical separation of hot and cold thermoreceptors at the periphery results in “labeled lines” for hot and cold which are interpreted largely independently to produce temperature preference behavior.

## DISCUSSION

### A Conserved Logic for Encoding Temperature Information at the Periphery

The *Drosophila* antenna is a remarkable “hub” for the fly's senses, housing cells specialized in detecting sound, humidity, wind direction, gravity, pheromone and olfactory cues ([Ha and Smith, 2009](#); [Kamikouchi et al., 2009](#); [Liu et al., 2007](#); [Sun et al., 2009](#); [Vosshall and Stocker, 2007](#); [Yorozu et al., 2009](#)). Here, we show that the arista and sacculus, two unique structures in the antenna, contain thermoreceptors. The antennal thermosensory cells belong to two functional classes: one is activated by heating (hot receptors) and the other by cooling (cold receptors). Notably, each cell type undergoes not only a rapid, transient increase in calcium responses to the cognate stimulus, but in addition a rapid  $[Ca^{2+}]_i$  drop to the opposite one (i.e., heat for cold cells and cooling for hot cells). Both

Center (AMMC; data not shown; the scalebar represents 50  $\mu$ m; see also [Figure S4](#)).

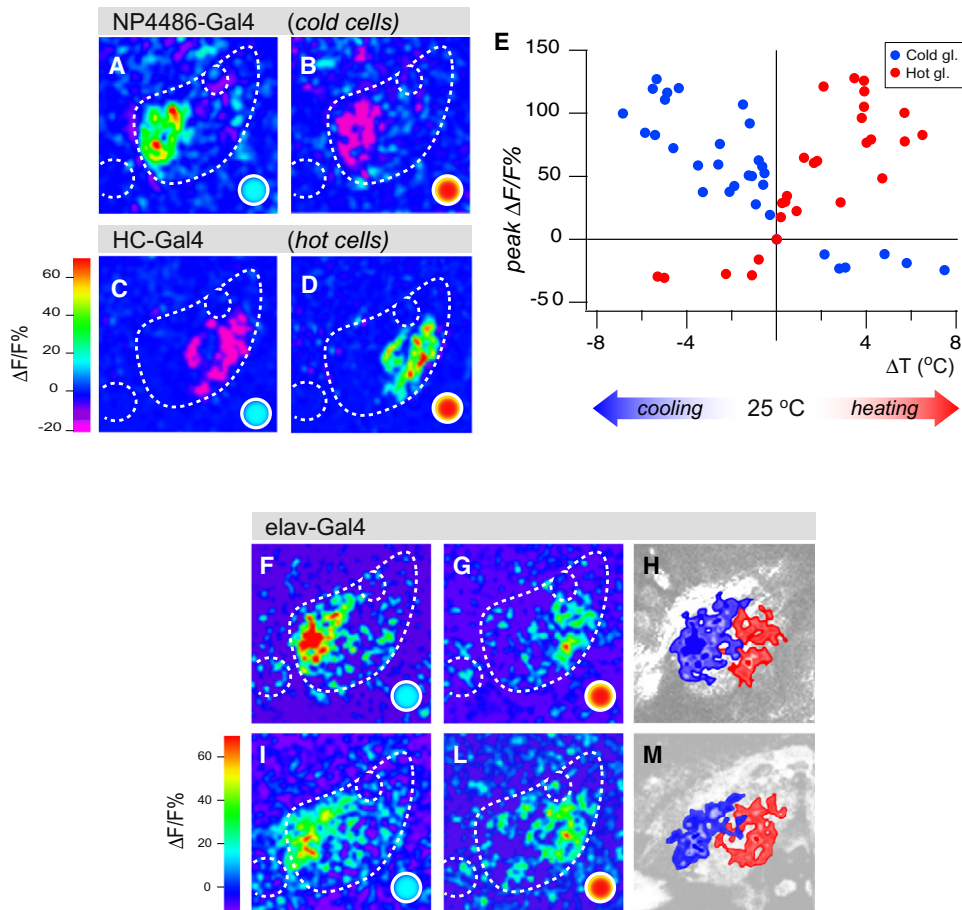


**Figure 5. A Map of Temperature in the PAP**

(A–E) (A) Cold stimulation elicits robust calcium increases in the “cold” glomerulus, while (B) hot stimulation results in a specific decrease in  $\text{Ca}^{2+}$ . Conversely, (C) the “hot” glomerulus is inhibited by cold stimuli, and (D) activated by hot ones; hot and cold stimuli were  $\Delta t \sim 5^\circ\text{C}$  from  $\sim 25^\circ\text{C}$  (red spot: hot stimulus; blue spot: cold stimulus; G-CaMP was driven under the control of HC-Gal4 or NP4486-Gal4, respectively). (E) Stimulus-response plot representing the responses of “hot” (red dots) and “cold” (blue dots) glomeruli. The responses are proportional to the magnitude of the temperature change, with “hot” glomeruli increasing G-CaMP fluorescence in response to heating stimuli and decreasing it upon cooling. Vice versa, “cold” glomeruli are activated by cooling and appear inhibited by heating stimuli (heating or cooling was from  $25^\circ\text{C}$ ; each dot represents the response of a single glomerulus to a stimulus; each animal expressed G-CaMP under the control of HC-Gal4 or NP4486-Gal4, and was subjected to a maximum of 3 stimuli of different intensity, see Experimental Procedures for details,  $n = 10$ ). (F–M) A similar pattern of activity is recorded in the PAP when G-CaMP is expressed throughout the brain using a pan-neuronal driver (elav-Gal4); two independent experiments in two different animals are shown. Note the segregation in the response to “cold” (F and I) versus “hot” (G and L) stimuli ( $\Delta t \sim 5^\circ\text{C}$  from  $25^\circ\text{C}$ ). Panels (H and M) are schematic drawings of the superimposed responses in each animal (see also Figure S5).

classes of neurons respond with high sensitivity to small temperature changes ( $<0.5^\circ\text{C}$ ), and their calcium transients scale well with the magnitude of the change, particularly for small stimuli ( $\Delta t < 5^\circ\text{C}$ ). Thus, these cells are likely to report most accurately the direction and magnitude of small, sudden changes in temperature. Given that flies are poikilotherms, detecting and reacting to changes in temperature with high sensitivity and speed is vital to the survival of the animal.

Mammalian warm and cold thermoreceptive skin fibers are characterized by robust spontaneous activity (which scale with the absolute temperature over a rather broad range), and respond with an abrupt increase in firing rate to either a sudden increase (hot receptors) or to a sudden decrease (cold receptors) in temperature. Interestingly, their resting firing rate decreases sharply when challenged by the opposite thermal stimulus

(Darian-Smith, 1971; Hensel, 1981). The fly antennal thermosensors appear to have similar properties, with the caveat that G-CaMP imaging does not allow us to monitor resting firing rates, but rather changes in spiking frequency. Thus, we suggest that mammals and flies might use a remarkably similar strategy to encode temperature stimuli at the periphery: the activity of specifically tuned populations of cells signals the direction of the temperature change (hot and cold receptors), and the degree to which they are activated signals the intensity of the change (Lumpkin and Caterina, 2007).

#### Labeled Lines and a Map of Temperature in the Protocerebrum

How is the peripheral temperature “code” represented in the fly brain? The ability to selectively label defined populations of

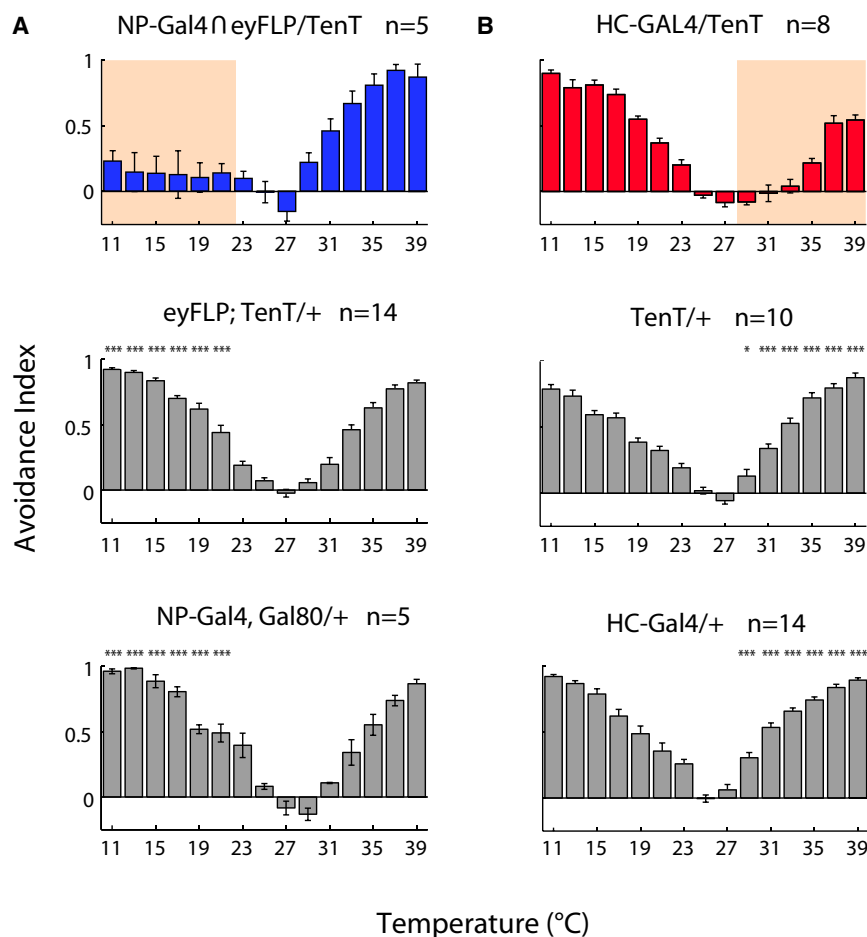


**Figure 6. Labeled Lines for Temperature Processing**

(A and B) The behavioral effects of the inactivation of cold and hot thermoreceptors reveal separate channels for the processing of cold and hot temperatures. (A) Expression of tetanus toxin in antennal cold receptors results in significant loss of aversion for temperatures in the 11°C–23°C range. In contrast, (B) inactivation of hot receptors results in the reciprocal phenotype, a selective loss of aversion to temperatures above 29°C. Shown below each experimental genotype are the thermal preference records for the parental control lines (gray bars). Pink shading in (A) and (B) highlights AI values significantly different from both appropriate parental strains ( $n > 5$ , mean  $\pm$  SEM; \*\*\* =  $p < 0.001$ , \*\* =  $p < 0.01$ , \* =  $p < 0.05$ , ANOVA, see [Experimental Procedures](#) for details).

model predicts that altering one of the lines should not affect the behavioral response to the other: such manipulation would just re-define the boundaries for the preferred temperature. For example a loss of the cold line would produce flies which are no longer averse to temperatures below 21°C, but still retain the 28°C warm limit. Indeed, this is precisely what was observed, suggesting that the preferred temperature may in fact be set by the independent action of each receptor system. Together, these results substantiate a thermotopic map in the fly brain, suggest a “labeled line” organization for temperature sensing, and illustrate how dedicated temperature signals from two independent and opposing sensors (hot and cold receptors) can direct behavior.

neurons allowed us to track the projections of the antennal hot and cold receptors directly into the brain, and to image their activity in response to temperature stimuli. Our results showed that the axons of these neurons converge into anatomically and functionally distinct glomeruli in the Proximal Antennal Protocerebrum (PAP). Thus, temperature, like the five classical senses, is represented in a defined brain locus by a spatial map of activity.

Given the segregation of hot and cold signals in the PAP, how do flies choose their preferred temperature to orchestrate behavior? We envision at least two potential scenarios: in one, information from both lines (i.e., hot and cold) is combined somewhere upstream of the PAP to decode temperature signals, generate a temperature reading and trigger the appropriate behavioral responses. Alternatively, the “preferred temperature” might be a default state, in essence a point (or temperature range) defined by the independent activity of two labeled lines each mediating behavioral aversion to temperatures above or below this point (in this case temperatures below 21°C and above 28°C). This push-push mechanism would de-mark the boundaries of the non-aversive (i.e., preferred) temperature range, and thus provide a very robust mechanism for transforming temperature signals into a simple behavioral choice. This

illustrate how dedicated temperature signals from two independent and opposing sensors (hot and cold receptors) can direct behavior.

## EXPERIMENTAL PROCEDURES

### Experimental Animals and Transgenes

The *brv1* NP4486 allele is from the Gal4 enhancer trap database at the DGRC, Kyoto Institute of Technology (Hayashi et al., 2002). It harbors a single, P(GawB) insert 2,249 bp downstream of the CG9472 STOP codon (Hayashi et al., 2002). A single early termination mutation was identified for each *brv1* and *brv2* by Tilling (McCallum et al., 2000): for *brv1* the nucleotide change was T > A at position 1683 from the START codon, resulting in the L563 > STOP change in the protein sequence. For *brv2*, we recovered a G > A change at position 754 from the START codon, resulting in the early termination W205 > STOP. The temperature preference phenotype of each mutant was also tested *in trans* to a deletion uncovering the region (Df(3L)Exel9007 for *brv1* and Df(3L)Exel6131 for *brv2*) and was indistinguishable from that of homozygous mutants (Figure S1 and data not shown): we conclude that these alleles are likely null or strong loss of function mutations. The *brv2* rescue construct was produced by cloning a 4 Kb genomic fragment including the *brv2* coding region into a modified pCasper vector. The hot-cell Gal4 driver line was identified from a collection covering a wide range of candidates with expression in the antennae (Hayashi et al., 2002; flybase.org; pubmed.org). To restrict expression of CD8:GFP and TeNT to antennal neurons expressing NP4486, we used the following intersectional strategy: eyFLP is



active in the antenna (and in the retina), but not in the brain. *tubP-FRT > Gal80 > FRT* drives expression of the Gal4 inhibitor Gal80 ubiquitously, effectively silencing NP4486-Gal4 mediated expression of the transgenes. Only in the antenna, where *eyFLP* is active, the *FRT > Gal80 > FRT* cassette is excised and lost, allowing Gal4-mediated expression. This effectively limits transgene expression to the cells in which both *eyFLP* and NP4486 are active.

### Behavioral Assays

All assays were carried out in a room kept at  $\sim 24^{\circ}\text{C}$ ,  $\sim 40\%$  RH. The temperature gradient arena has been previously described (Sayeed and Benzer, 1996) (Figure S1). For two choice assays (Figure 1 and Figure 6) 15 flies are placed on an arena consisting of four 1" square, individually addressable Peltier tiles (Oven Industries Inc.). In each trial, flies are presented for 3' with a choice between  $25^{\circ}\text{C}$  and a test temperature between 11 and  $39^{\circ}\text{C}$  at  $2^{\circ}\text{C}$  intervals (15 trials total). The position of flies is monitored during each trial to calculate an avoidance index for each test temperature. The avoidance index is defined as  $(\text{AI} = \# \text{flies at } 25^{\circ}\text{C} - \# \text{flies at test temp}) / \text{total } \# \text{flies}$ . AI values were compared using t tests (Figures S1A and S1B) or by 2-way ANOVA followed by Bonferroni post-tests when comparing more than 2 groups (Figure 1, Figure S1, and Figure 6). Kolmogorov-Smirnov tests were used to confirm a normally distributed sample. Threshold  $p = 0.05$ . Constant variance of the datasets was also confirmed by computing the Spearman rank correlation between the absolute values of the residuals and the observed value of the dependent variable, by SigmaPlot).

### In Situ Hybridization and Immunohistochemistry

Fluorescent in situ hybridization was carried out as in (Benton et al., 2006) with a *brv1* digoxigenin-labeled RNA probe visualized with sheep anti-digoxigenin (Boehringer), followed by donkey anti-sheep Cy3 (Jackson). We were unable to detect *brv2* or *brv3* expression by ISH. Immunohistochemistry was performed using standard protocols.

### Real-Time PCR

Quantitative PCR was carried out in quintuplicates using Brilliant SYBR Green PCR Master Mix (Stratagene) on a StepOnePlus real-time PCR system (Applied Biosystems) using *brv3* specific primers. Beta-actin served as the endogenous normalization control.

### Live Imaging and Two-Photon Microscopy

Confocal Images were obtained using a Zeiss LSM510 confocal microscope with an argon-krypton laser. For live imaging through the cuticle, intact heads or whole flies were mounted within a custom-built perfusion chamber covered with a coverslip and imaged through a water-immersion 40X Zeiss objective and a EM-CCD camera (Photonmax, Princeton Instruments). Image series were acquired at 10 frames per second and analyzed using ImageJ and a custom macro written in Igor Pro (Wavemetrics). To image the responses of cold receptor neurons in *brv1* and -2 mutant backgrounds (Figure 2), G-CaMP was expressed in all arista neurons (under *elav-Gal4*) in controls (background-matched) and mutant animals. At the beginning of each experiment, a set of defined hot and cold stimuli ( $\Delta t \sim 3^{\circ}\text{C}$ ) was delivered while imaging on different focal planes to identify the 3 hot and 3 cold cells in each arista (note that the G-CaMP responses of hot cells -including inhibition to cold stimuli- remain normal in *brv1* and -2 backgrounds). The most optically accessible cold receptor cell in each arista was then imaged responding to various cold stimuli. A maximum of 5 stimuli of different intensities was recorded for each preparation.

For two-photon microscopy, we built a customized system based on a Movable Objective Microscope (MOM) from Sutter (Sutter Inc.) in combination with a ultrafast Ti:Sapphire laser from Coherent (Chameleon). Live imaging experiments were captured at four frames per second with a resolution of  $128 \times 128$  pixels. Analysis of imaging data and  $\Delta F/F$  calculations were performed using Igor Pro and a custom macro as in (Wang et al., 2003). For live imaging of PAP projections, fly heads were immobilized in a custom built perfusion chamber. Sufficient head cuticle and connective tissue was removed to allow optical access to the PAP. Temperature stimulation was achieved by controlling the temperature of the medium, constantly flowing

over the preparation at 5ml/min, by a custom-built system of 3 way valves (Lee Instruments, response time 2ms). In all experiments, heating or cooling was at  $\sim 1^{\circ}\text{C}/\text{sec}$ . Temperature was recorded using a BAT-12 electronic thermometer equipped with a custom microprobe (time constant .004 s, accuracy  $0.01^{\circ}\text{C}$ , Physitemp).

### SUPPLEMENTAL INFORMATION

Supplemental Information includes Extended Experimental Procedures and five figures and can be found with this article online at doi:10.1016/j.cell.2011.01.028.

### ACKNOWLEDGMENTS

We thank Cahir O'Kane for UAS-TeNT flies; Paul Garrity for dTRPA1<sup>KO</sup> flies; and especially Michael Reiser for invaluable help with designing and implementing the behavioral arenas and assays. We also thank David Julius and Avi Priel for their help and kindness hosting us (M.G.) in our efforts to express Brv channels in *Xenopus* oocytes. Wilson Kwan, George Gallardo, and Lisa Ha provided expert help with fly husbandry. We are grateful to Hojoon Lee, Dimitri Trankner, and Robert Barretto for help with experiments and data analysis; and Nick Ryba, Michael Reiser, and members of the Zuker lab for critical comments on the manuscript. We also thank Kevin Moses, Gerry Rubin, and the Janelia Farm Visitor Program. M.G. was supported by a Wenner-Grens Stiftelse and a Human Frontiers Science Program long term fellowship. L.J.M. is a fellow of the Jane Coffin Childs Foundation. C.S.Z. is an investigator of the Howard Hughes Medical Institute and a Senior Fellow at Janelia Farm Research Campus. Author contributions: M.G. and C.S.Z. conceived all the experiments and wrote the paper. M.G. performed all the experiments presented in this paper, except the in situ hybridizations (T.A.O.). T.A.O. also helped with the set up for 2-choice behavioral assays, and J.W.W. helped design and setup the custom imaging system. L.J.M., M.G., and T.A.O. carried out extensive efforts to heterologously express Brv channels (data not shown).

Received: February 17, 2010

Revised: November 3, 2010

Accepted: January 24, 2011

Published: February 17, 2011

### REFERENCES

- Altner, H., and Loftus, R. (1985). Ultrastructure and Function of Insect Thermo- And Hygroreceptors doi:10.1146/annurev.en.30.010185.001421. Annual Review of Entomology 30, 273-295.
- Basbaum, A.I., Bautista, D.M., Scherrer, G., and Julius, D. (2009). Cellular and molecular mechanisms of pain. *Cell* 139, 267-284.
- Bateman, A., Birney, E., Durbin, R., Eddy, S.R., Howe, K.L., and Sonnhammer, E.L. (2000). The Pfam protein families database. *Nucleic Acids Res.* 28, 263-266.
- Bautista, D.M., Siemens, J., Glazer, J.M., Tsuruda, P.R., Basbaum, A.I., Stucky, C.L., Jordt, S.E., and Julius, D. (2007). The menthol receptor TRPM8 is the principal detector of environmental cold. *Nature* 448, 204-208.
- Benton, R., Sachse, S., Michnick, S.W., and Vosshall, L.B. (2006). Atypical membrane topology and heteromeric function of *Drosophila* odorant receptors in vivo. *PLoS Biol.* 4, e20.
- Buchner, E., Bader, R., Buchner, S., Cox, J., Emson, P.C., Flory, E., Heizmann, C.W., Hemm, S., Hofbauer, A., and Oertel, W.H. (1988). Cell-specific immunoprobe for the brain of normal and mutant *Drosophila melanogaster*. I. Wild-type visual system. *Cell Tissue Res.* 253, 357-370.
- Caterina, M.J., Leffler, A., Malmberg, A.B., Martin, W.J., Trafton, J., Petersen-Zeit, K.R., Koltzenburg, M., Basbaum, A.I., and Julius, D. (2000). Impaired nociception and pain sensation in mice lacking the capsaicin receptor. *Science* 288, 306-313.

- Caterina, M.J., Rosen, T.A., Tominaga, M., Brake, A.J., and Julius, D. (1999). A capsaicin-receptor homologue with a high threshold for noxious heat. *Nature* 398, 436–441.
- Caterina, M.J., Schumacher, M.A., Tominaga, M., Rosen, T.A., Levine, J.D., and Julius, D. (1997). The capsaicin receptor: a heat-activated ion channel in the pain pathway. *Nature* 389, 816–824.
- Colburn, R.W., Lubin, M.L., Stone, D.J., Jr., Wang, Y., Lawrence, D., D'Andrea, M.R., Brandt, M.R., Liu, Y., Flores, C.M., and Qin, N. (2007). Attenuated Cold Sensitivity in TRPM8 Null Mice. *Neuron* 54, 379–386.
- Darian-Smith, I.D.R.W. (1971). *Peripheral neural mechanisms of thermal sensation* (New York: Appleton-Century Crofts Meredith Corp.).
- Denk, W., Strickler, J.H., and Webb, W.W. (1990). Two-photon laser scanning fluorescence microscopy. *Science* 248, 73–76.
- Dhaka, A., Earley, T.J., Watson, J., and Patapoutian, A. (2008). Visualizing cold spots: TRPM8-expressing sensory neurons and their projections. *J. Neurosci.* 28, 566–575.
- Dhaka, A., Murray, A.N., Mathur, J., Earley, T.J., Petrus, M.J., and Patapoutian, A. (2007). TRPM8 Is Required for Cold Sensation in Mice. *Neuron* 54, 371–378.
- Foelix, R.F., Stocker, R.F., and Steinbrecht, R.A. (1989). Fine structure of a sensory organ in the arista of *Drosophila melanogaster* and some other dipterans. *Cell Tissue Res.* 258, 277–287.
- Guler, A.D., Lee, H., Iida, T., Shimizu, I., Tominaga, M., and Caterina, M. (2002). Heat-evoked activation of the ion channel, TRPV4. *J. Neurosci.* 22, 6408–6414.
- Ha, T.S., and Smith, D.P. (2009). Odorant and pheromone receptors in insects. *Front Cell Neurosci* 3, 10.
- Hamada, F.N., Rosenzweig, M., Kang, K., Pulver, S.R., Ghezzi, A., Jegla, T.J., and Garrity, P.A. (2008). An internal thermal sensor controlling temperature preference in *Drosophila*. *Nature* 454, 217–220.
- Hayashi, S., Ito, K., Sado, Y., Taniguchi, M., Akimoto, A., Takeuchi, H., Aigaki, T., Matsuzaki, F., Nakagoshi, H., Tanimura, T., et al. (2002). GETDB, a database compiling expression patterns and molecular locations of a collection of Gal4 enhancer traps. *Genesis* 34, 58–61.
- Hensel, H. (1981). *Thermoreception and Temperature Regulation* (London: Academic Press).
- Jordt, S.E., McKemy, D.D., and Julius, D. (2003). Lessons from peppers and peppermint: the molecular logic of thermosensation. *Curr. Opin. Neurobiol.* 13, 487–492.
- Kamikouchi, A., Inagaki, H.K., Effertz, T., Hendrich, O., Fiala, A., Gopfert, M.C., and Ito, K. (2009). The neural basis of *Drosophila* gravity-sensing and hearing. *Nature* 458, 165–171.
- Kobayashi, K., Fukuoka, T., Obata, K., Yamanaka, H., Dai, Y., Tokunaga, A., and Noguchi, K. (2005). Distinct expression of TRPM8, TRPA1, and TRPV1 mRNAs in rat primary afferent neurons with  $\delta$ /c-fibers and colocalization with trk receptors. *J. Comp. Neurol.* 493, 596–606.
- Koundakjian, E.J., Cowan, D.M., Hardy, R.W., and Becker, A.H. (2004). The Zuker collection: a resource for the analysis of autosomal gene function in *Drosophila melanogaster*. *Genetics* 167, 203–206.
- Kwon, Y., Shim, H.S., Wang, X., and Montell, C. (2008). Control of thermotactic behavior via coupling of a TRP channel to a phospholipase C signaling cascade. *Nat. Neurosci.* 11, 871–873.
- Lee, H., Iida, T., Mizuno, A., Suzuki, M., and Caterina, M.J. (2005). Altered thermal selection behavior in mice lacking transient receptor potential vanilloid 4. *J. Neurosci.* 25, 1304–1310.
- Lin, D.M., and Goodman, C.S. (1994). Ectopic and increased expression of Fasciclin II alters motoneuron growth cone guidance. *Neuron* 13, 507–523.
- Liu, L., Li, Y., Wang, R., Yin, C., Dong, Q., Hing, H., Kim, C., and Welsh, M.J. (2007). *Drosophila* hygrosensation requires the TRP channels water witch and nanchung. *Nature* 450, 294–298.
- Lumpkin, E.A., and Caterina, M.J. (2007). Mechanisms of sensory transduction in the skin. *Nature* 445, 858–865.
- McCallum, C.M., Comai, L., Greene, E.A., and Henikoff, S. (2000). Targeted screening for induced mutations. *Nat. Biotechnol.* 18, 455–457.
- McKemy, D.D. (2007). Temperature sensing across species (Pflugers Arch).
- McKemy, D.D., Neuhausser, W.M., and Julius, D. (2002). Identification of a cold receptor reveals a general role for TRP channels in thermosensation. *Nature* 416, 52–58.
- Montell, C., Birnbaumer, L., Flockerzi, V., Bindels, R.J., Bruford, E.A., Caterina, M.J., Clapham, D.E., Harteneck, C., Heller, S., Julius, D., et al. (2002). A unified nomenclature for the superfamily of TRP cation channels. *Mol. Cell* 9, 229–231.
- Moqrich, A., Hwang, S.W., Earley, T.J., Petrus, M.J., Murray, A.N., Spencer, K.S., Andahazy, M., Story, G.M., and Patapoutian, A. (2005). Impaired thermosensation in mice lacking TRPV3, a heat and camphor sensor in the skin. *Science* 307, 1468–1472.
- Nakai, J., Ohkura, M., and Imoto, K. (2001). A high signal-to-noise Ca<sup>2+</sup> probe composed of a single green fluorescent protein. *Nat. Biotechnol.* 19, 137–141.
- Ni, J.Q., Liu, L.P., Binari, R., Hardy, R., Shim, H.S., Cavallaro, A., Booker, M., Pfeiffer, B.D., Markstein, M., Wang, H., et al. (2009). A *Drosophila* resource of transgenic RNAi lines for neurogenetics. *Genetics* 182, 1089–1100.
- Patapoutian, A., Peier, A.M., Story, G.M., and Viswanath, V. (2003). ThermoTRP channels and beyond: mechanisms of temperature sensation. *Nat. Rev. Neurosci.* 4, 529–539.
- Peier, A.M., Moqrich, A., Hergarden, A.C., Reeve, A.J., Andersson, D.A., Story, G.M., Earley, T.J., Dragoni, I., McIntyre, P., Bevan, S., et al. (2002a). A TRP channel that senses cold stimuli and menthol. *Cell* 108, 705–715.
- Peier, A.M., Reeve, A.J., Andersson, D.A., Moqrich, A., Earley, T.J., Hergarden, A.C., Story, G.M., Colley, S., Hogenesch, J.B., McIntyre, P., et al. (2002b). A heat-sensitive TRP channel expressed in keratinocytes. *Science* 296, 2046–2049.
- Plant, T.D., and Strotmann, R. (2007). Trpv4. *Handb Exp Pharmacol.* 189–205.
- Roark, M., Sturtevant, M.A., Emery, J., Vaessin, H., Grell, E., and Bier, E. (1995). scratch, a pan-neural gene encoding a zinc finger protein related to snail, promotes neuronal development. *Genes Dev.* 9, 2384–2398.
- Root, C.M., Semmelhack, J.L., Wong, A.M., Flores, J., and Wang, J.W. (2007). Propagation of olfactory information in *Drosophila*. *Proc. Natl. Acad. Sci. USA* 104, 11826–11831.
- Rosenzweig, M., Brennan, K.M., Tayler, T.D., Phelps, P.O., Patapoutian, A., and Garrity, P.A. (2005). The *Drosophila* ortholog of vertebrate TRPA1 regulates thermotaxis. *Genes Dev.* 19, 419–424.
- Sayeed, O., and Benzer, S. (1996). Behavioral genetics of thermosensation and hygrosensation in *Drosophila*. *Proc. Natl. Acad. Sci. USA* 93, 6079–6084.
- Smith, G.D., Gunthorpe, M.J., Kelsell, R.E., Hayes, P.D., Reilly, P., Facer, P., Wright, J.E., Jerman, J.C., Walhin, J.P., Ooi, L., et al. (2002). TRPV3 is a temperature-sensitive vanilloid receptor-like protein. *Nature* 418, 186–190.
- Sokabe, T., Tsujiuchi, S., Kadowaki, T., and Tominaga, M. (2008). *Drosophila* painless is a Ca<sup>2+</sup>-requiring channel activated by noxious heat. *J. Neurosci.* 28, 9929–9938.
- Story, G.M., Peier, A.M., Reeve, A.J., Eid, S.R., Mosbacher, J., Hricik, T.R., Earley, T.J., Hergarden, A.C., Andersson, D.A., Hwang, S.W., et al. (2003). ANKTM1, a TRP-like channel expressed in nociceptive neurons, is activated by cold temperatures. *Cell* 112, 819–829.
- Sun, Y., Liu, L., Ben-Shahar, Y., Jacobs, J.S., Eberl, D.F., and Welsh, M.J. (2009). TRPA channels distinguish gravity sensing from hearing in Johnston's organ. *Proc. Natl. Acad. Sci. USA* 106, 13606–13611.
- Sweeney, S.T., Brodie, K., Keane, J., Niemann, H., and O'Kane, C.J. (1995). Targeted expression of tetanus toxin light chain in *Drosophila* specifically eliminates synaptic transmission and causes behavioral defects. *Neuron* 14, 341–351.
- Takashima, Y., Daniels, R.L., Knowlton, W., Teng, J., Liman, E.R., and McKemy, D.D. (2007). Diversity in the neural circuitry of cold sensing revealed by genetic axonal labeling of transient receptor potential melastatin 8 neurons. *J. Neurosci.* 27, 14147–14157.

- Till, B.J., Colbert, T., Tompa, R., Enns, L.C., Codomo, C.A., Johnson, J.E., Reynolds, S.H., Henikoff, J.G., Greene, E.A., Steine, M.N., et al. (2003). High-throughput TILLING for functional genomics. *Methods Mol. Biol.* 236, 205–220.
- Tracey, W.D., Jr., Wilson, R.I., Laurent, G., and Benzer, S. (2003). *painless*, a *Drosophila* gene essential for nociception. *Cell* 113, 261–273.
- Viswanath, V., Story, G.M., Peier, A.M., Petrus, M.J., Lee, V.M., Hwang, S.W., Patapoutian, A., and Jegla, T. (2003). Opposite thermosensor in fruitfly and mouse. *Nature* 423, 822–823.
- Vosshall, L.B., and Stocker, R.F. (2007). Molecular architecture of smell and taste in *Drosophila*. *Annu. Rev. Neurosci.* 30, 505–533.
- Wang, J.W., Wong, A.M., Flores, J., Vosshall, L.B., and Axel, R. (2003). Two-photon calcium imaging reveals an odor-evoked map of activity in the fly brain. *Cell* 112, 271–282.
- Xu, H., Ramsey, I.S., Kotecha, S.A., Moran, M.M., Chong, J.A., Lawson, D., Ge, P., Lilly, J., Silos-Santiago, I., Xie, Y., et al. (2002). TRPV3 is a calcium-permeable temperature-sensitive cation channel. *Nature* 418, 181–186.
- Yorozu, S., Wong, A., Fischer, B.J., Dankert, H., Kernan, M.J., Kamikouchi, A., Ito, K., and Anderson, D.J. (2009). Distinct sensory representations of wind and near-field sound in the *Drosophila* brain. *Nature* 458, 201–205.
- Zars, T. (2001). Two thermosensors in *Drosophila* have different behavioral functions. *J. Comp. Physiol. [A]* 187, 235–242.

## EXTENDED EXPERIMENTAL PROCEDURES

### Experimental Animals and Transgenes

Flies were raised on standard medium at 25°C unless otherwise specified. The Canton-S strain was used as wild-type and an isogenic *bw, st* strain (Koundakjian et al., 2004) was used as a control for TILLING mutant lines (see below). To identify molecular null mutations for *brv1* and -2, we screened ~6000 EMS mutagenized F3 lines from the 3d chromosome Zuker collection (Koundakjian et al., 2004), through the Fly-TILL service (Till et al., 2003). TILLING (McCallum et al., 2000), is a high throughput molecular screening strategy to identify point mutations in target genes. In essence, DNA from each line is examined for the presence of nucleotide changes in a gene of interest (i.e., as compared to the parental controls). Primers for Tilling were selected to target a highly conserved stretch of coding DNA and were as follows: *brv1*, Left primer: CTTCTGTGTTCACTGAGCGGGACTTT. Right primer: CCTCAGTCTCTGGAACCTGCTCGTCTT. *brv2*, Left primer: AATACCAACAACATGCAGCGCCTCTTC. Right primer: GGAAGAAATCCGCAGGATGAATGTCAC. The *brv2* rescue construct was produced by cloning a 4 Kb genomic fragment including the *brv2* coding region into a modified pCasper vector as follows: specific genomic primers (SP, CTGCAGACCGGCGGATTTTA. ASP, AGAATCGCCGTAGCACAGGA) were modified by the addition of a NotI restriction site. The NotI-digested PCR product was then cloned into the Casper vector, which was used to produce transgenic flies. Additional lines used: UAS-*brv3* RNAi (Ni et al., 2009), *scratch-Gal4* (Roark et al., 1995), *elav-Gal4* (Lin and Goodman, 1994), UAS-CD8:GFP, UAS-NLS:GFP, UAS-syb:GFP (listed in fly-base: [www.fruitfly.org](http://www.fruitfly.org)), UAS-G-CaMP (Wang et al., 2003) (normally used in multiple copies to maximize expression), dTRPA1<sup>KO</sup> (Hamada et al., 2008), *eyFLP*, *tubP-FRT* > *Gal80* > *FRT* (Root et al., 2007), UAS- *TeNT* (Sweeney et al., 1995).

### Behavioral Assays

For all behavioral experiments, flies were aged for 5 days on a 16 hr light/ 8 hr dark circadian cycle. In all cases involving Gal4 driven transgenes (i.e., *brv3* RNAi and toxin experiments), experimental genotypes and controls were grown and aged at 29°C to maximize transgene expression. All assays were carried out in a room kept at ~24°C, ~40% RH. The temperature gradient arena (Sayeed and Benzer, 1996) Figure S1) consists of a 50 cm long aluminum block with a temperature gradient between 18 and 29°C. In each experiment groups of 100 flies are allowed to distribute on the gradient. After 30 min, the location of each fly is recorded by a digital camera (pixelink) and plotted as a function of the gradient's temperature; the resulting population distribution is then used as that line's thermal preference. For two choice assays (Figure 1 and Figure 6) 15 flies are placed on an arena consisting of four 1" square, individually addressable Peltier tiles (Oven Industries Inc.) calibrated using a thermal imaging system (OptoTherm Inc.). In each trial, flies are presented with a choice between 25°C and a test temperature between 11 and 39°C at 2°C intervals (15 trials total). At the beginning of each trial, flies are dispersed by raising the temperature of all four tiles to 33°C for 20 s. Next, two tiles are set to 25°C and two at a test temperature between 11 and 39°C (the flies encounter a consistent temperature stimulus, as they are kept under a glass layer coated with Sigmacote (Sigma-Aldrich, Inc.), preventing them from escaping the temperature-controlled floor tiles). Fly location is recorded continuously for 3 min using a CMOS camera (BASLER A622f). Next, the temperatures of the 4 tiles are reversed for a 3 min re-test. Following the re-test, a new trial is initiated until all 15 temperature comparisons have been performed. The videos are analyzed off-line using a custom Matlab script to calculate an avoidance index for each test temperature. The avoidance index is defined as  $(AI = \#flies\ at\ 25^\circ C - \#flies\ at\ test\ temp) / total\ \#flies$ . The avoidance index is reported as the mean avoidance index in the period from 60 to 180 s of each temperature comparison.

### Cell Culture and Expression Studies

Attempts to functionally express *brv1*, -2, and -3 in mammalian (HEK293, COS, HeLa), *Xenopus* oocytes, and insect cells (T. Ni, Sf9, BG3c2) produced either sporadic (T. Ni) or negligible temperature responses (all others). We also mis-expressed *brv1* and -2 in vivo in *Drosophila* olfactory and taste neurons, but failed to elicit thermal sensitivity in those cells (assessed by live imaging with G-CaMP). We believe essential factors are likely required for functional expression in vivo (and in vitro) outside the context of the native cold-sensing neurons.

### In Situ Hybridization and Immunohistochemistry

Fluorescent in situ hybridization was carried out with a *brv1* digoxigenin-labeled RNA probe. The digoxigenin probe was visualized with sheep anti-digoxigenin (Boehringer) followed by donkey anti-sheep Cy3 (Jackson). Sections were mounted in Vectashield reagent (Vector Labs) and viewed on a Zeiss LSM510 laser scanning confocal microscope. We were unable to detect *brv2* or *brv3* expression by ISH. For immunohistochemistry, dissected fly brains where fixed in PBS containing 4% paraformaldehyde and 0.1% Triton X-100 for 1 hr on ice and subsequently rinsed in PBT (PBS, 0.1% Triton X-100) five times at room temperature. Blocking was performed for 1 hr in PBSBT (PBS, 0.2% Triton X-100, 3% BSA) and samples were incubated overnight at 4°C with the appropriate dilution of primary antibody in PBSBT. Following 5 washes in PBSBT, the samples were incubated for 3 hr with the appropriate dilution of secondary antibody in PBSBT. After 5 more washes in PBT, brains were mounted in Vectashield (Vector Labs) and imaged on a Zeiss LSM510 laser scanning confocal microscope. Antibodies used were: nc82 (1:30), mouse monoclonal (Buchner et al., 1988); chicken anti-GFP (1:1000, Abcam #13970). Secondaries: anti-Chicken 488 (1:1000, Jackson 703-485-155), anti-Mouse Cy3 (1:1000, Jackson 715-165-150).



### Real-Time PCR

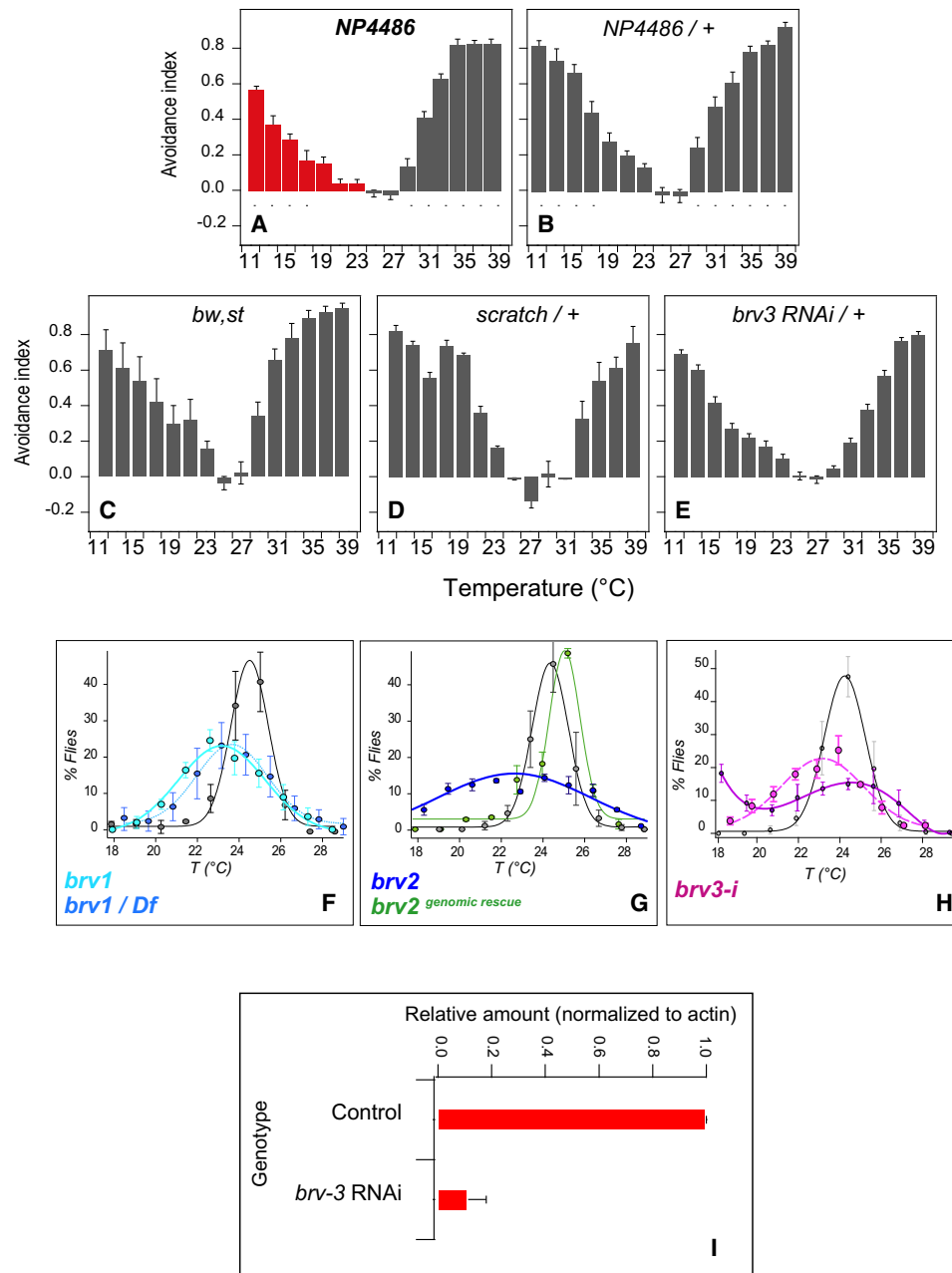
For quantitative PCR, fly heads from the appropriate genotypes were collected and frozen in liquid nitrogen. Total RNA was isolated using the RNeasy Micro kit (QIAGEN) according to the manufacturer's instructions. Equivalent amounts of total RNA served as template for cDNA synthesis with SuperscriptIII reverse transcriptase (Invitrogen). Quantitative PCR was carried out in quintuplicates using Brilliant SYBR Green PCR Master Mix (Stratagene) on a StepOnePlus real-time PCR system (Applied Biosystems). Primers were: TACAGCGTAAAGTCGATGAA (*brv3* -fwd); AGATGGGCTTTGAGTTCCTC (*brv3*-rev); CAGGCGGTGCTTTCTCTCTA ( $\beta$ -actin -fwd); AGCTGTAACCGCGCTCAGTA ( $\beta$ -actin -rev). Beta-actin served as the endogenous normalization control.

### Live Imaging and Two-Photon Microscopy

For imaging experiments, we used flies aged less than 3 days, as this appeared to reduce background fluorescence (Wang et al., 2003). For live confocal microscopy, intact tissues were visualized by exciting the tissue with blue light (488 nm) and collecting auto-fluorescence signals in the red (>600 nm) and GFP-fluorescence in the green channel (500-550 nm). Images were obtained using a Zeiss LSM510 confocal microscope with an argon-krypton laser. For live imaging through the cuticle, intact heads or whole flies were mounted within a small, custom-built perfusion chamber covered with a coverslip and imaged through a water-immersion 40X Zeiss objective and a EM-CCD camera (Photonmax, Princeton Instruments). Image series were acquired at 10 frames per second and analyzed using ImageJ and a custom macro written in Igor Pro (Wavemetrics). For two-photon microscopy, we used a system based on a Movable Objective Microscope (MOM) from Sutter (Sutter Inc.) in combination with an ultrafast Ti:Sapphire laser from Coherent (Chameleon). Live imaging experiments were captured at four frames per second with a resolution of 128 × 128 pixels. At the end of each experiment, a high-resolution z stack of images (512 × 512 pixels) was collected to aid in the identification of landmark brain structures. For live imaging of PAP projections, sufficient head cuticle and connective tissue had to be removed to allow optical access to the PAP. This was typically achieved by gently pulling forward the cuticular plate that houses the antennae, and pinning it in position without damaging the antennal nerves. Further pinning of head structures (air sacs, proboscis, cuticle) was also important to reduce tissue movement during perfusion and imaging. The chamber was then covered with a small coverslip and imaged using a water immersion 40X Zeiss objective. This preparation could respond to temperature stimulation for up to five hours. For all imaging experiments, the perfusion medium was an adult hemolymph like (AHL) saline containing 108 mM NaCl, 5 mM KCl, 2 mM CaCl<sub>2</sub>, 8.2 mM MgCl<sub>2</sub>, 4 mM NaHCO<sub>3</sub>, 1 mM NaH<sub>2</sub>PO<sub>4</sub>, 5 mM trehalose, 10 mM sucrose, 5 mM HEPES (pH 7.5), described in (Wang et al., 2003). Temperature stimulation was achieved by controlling the temperature of the medium, constantly flowing over the preparation at 5ml/min, by a custom-built system of 3 way valves (Lee Instruments, response time 2ms) electronically controlled by ad hoc software written in Labview (National Instruments).

### Bioinformatics

Sequences were obtained from GenBank at the National Center for Biotechnology Information (NCBI). The *Drosophila* Brvs form a small sub-cluster within the TRPP subfamily when all annotated ion channels encoded in the *Drosophila* genome are aligned to a large, representative set of annotated ion channels encoded in the mouse genome. To collect a representative set of annotated ion channels from mouse, the Pfam database (<http://pfam.sanger.ac.uk/>) was searched for all entries containing the "Ion Transporter" domain signature (PF00520). The "Ion Transporter" domain signature is found in sodium, potassium, and calcium ion channels. The phylogenetic relationship among the retrieved sequences was evaluated by using the neighbor joining method. Phylogenetic trees were then tested by bootstrap analysis with 1,000 replicates. In addition to the "Ion Transporter" domain (PF00520), Brv1, Brv2 and Brv3 also contain a "PKD channel" domain signature (PF08016). This domain is found in a small subset of the "Ion Transporter" domain-containing ion channels, and defines the cation channel region of PKD1 and PKD2 proteins. Brv protein topology was predicted using the TMAP (<http://bioinfo4.limbo.ifm.liu.se/tmap/index.html>), TMHMM (<http://www.cbs.dtu.dk/services/TMHMM-2.0/>) and TMPRED ([http://www.ch.embnet.org/software/TMPRED\\_form.html](http://www.ch.embnet.org/software/TMPRED_form.html)) servers.



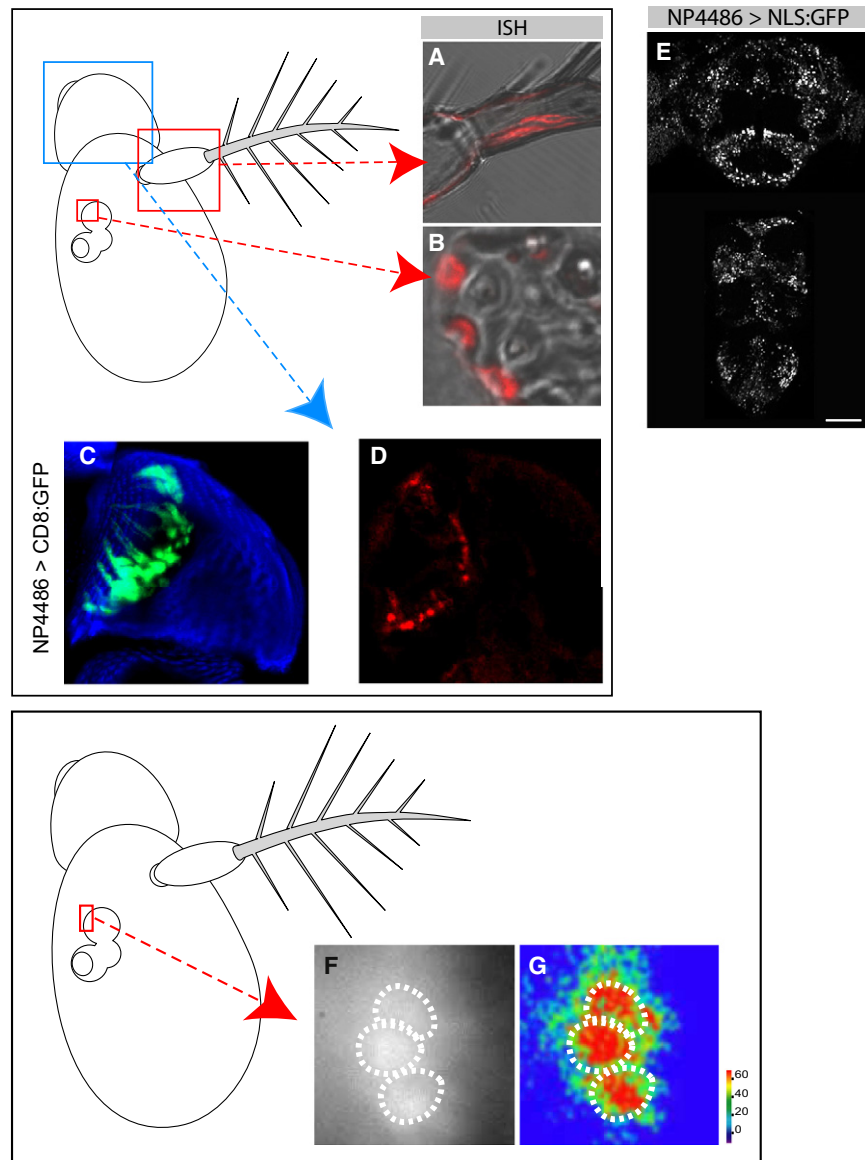


**Figure S2. Characterization of *brv1* Expression in the Antenna, and Additional Cold Receptors, Related to Figure 2**

*brv1* expression in antennae and CNS

(A–D) Schematic diagram of the antenna showing the sites of expression of *brv1*: (A, B, and D) In situ hybridization reveals *brv1* expression in (A) arista, (B) sacculus (red boxes), and (D) the second antennal segment (blue box). (C) Detail of the second antennal segment from a NP4486-Gal4 > CD8:GFP fly, showing the position of the *brv1* expressing mechanoreceptor neurons in the second segment (compare with the ISH in [D]).

(E) NP4486-Gal4 > UAS-NLS GFP reveals that NP4486-Gal4 is also active in scattered groups of neurons in the brain and ventral nerve chord. The panel shows a whole brain-VNC preparation, GFP was imaged live under a two-photon microscope (scalebar 50  $\mu$ m).

Cold receptors in the sacculus

(F and G) NP4486-expressing sacculus neurons respond to cooling stimuli. (F) Detail of 3 sacculus neurons expressing the calcium indicator G-CaMP under the control of NP4486-Gal4. (G) Maximal response of these cells to a stimulus of  $\sim\Delta t = 5^\circ\text{C}$  ( $\Delta F/F\%$  change is color coded).

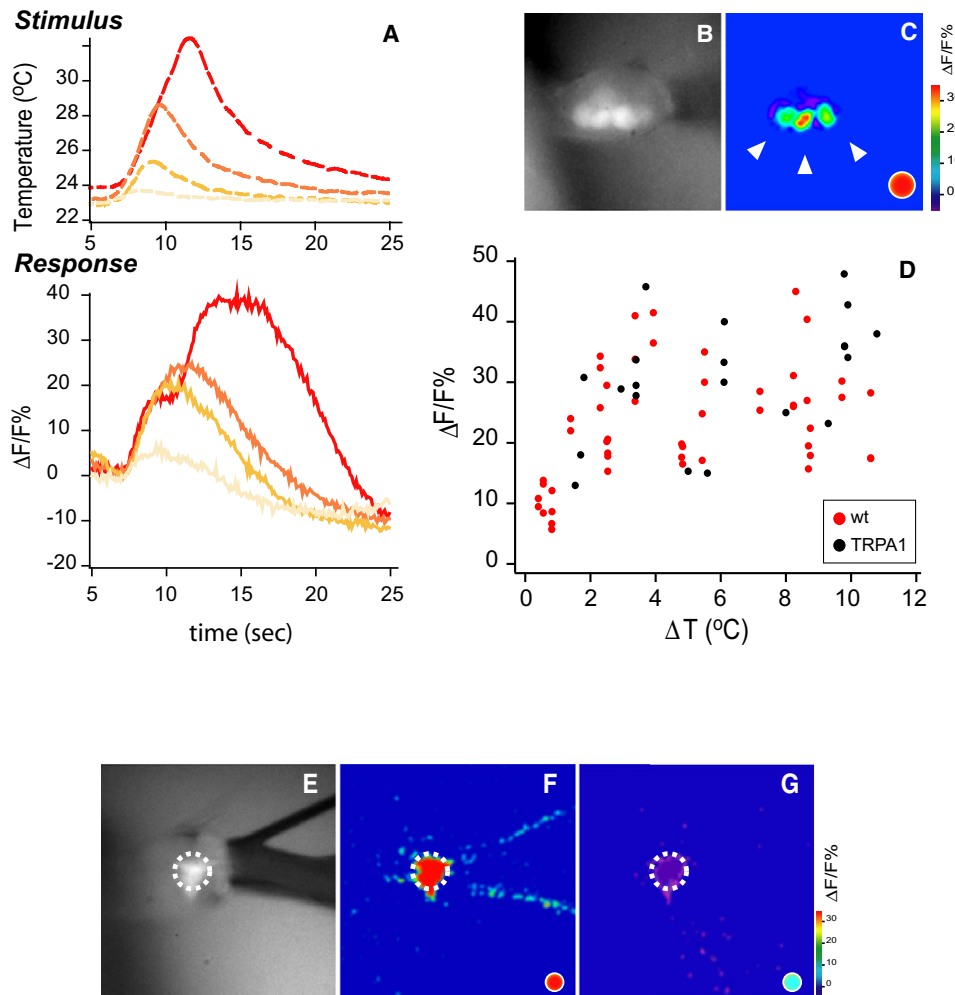


### Figure S3. Characterization of Hot Receptors, Related to Figure 3

Hot receptor responses in wild-type and dTRPA1 mutants

- (A–D) Calcium responses of arista hot thermoreceptors to heating stimuli. (A) Heating stimuli and the corresponding  $\text{Ca}^{2+}$  responses are shown for a single arista neuron expressing G-CaMP. Traces are color-coded such that each heating stimulus trace (above) is represented in the same color as the corresponding G-CaMP response (below) (B) Basal fluorescence image showing G-CaMP expression in all arista neurons driven by elav-Gal4; four arista neurons are visible in the focal plane (C) G-CaMP responses to a single hot stimulus ( $\Delta t \sim 5^\circ\text{C}$ ). Three arista hot receptors respond with a calcium increase to heating (arrowheads). (D) Stimulus/response plot for heating stimuli of varying intensity (red dots, wild-type). TRPA1-KO mutant responses are indistinguishable from wild-type (black dots). HC-Gal4 is expressed in hot but not cold temperature receptors in the arista
- (E) G-CaMP expression in the arista driven by HC-Gal4: a single cell is visible in the focal plane.
- (F) Maximal response to a hot stimulus of  $\sim \Delta t = 5^\circ\text{C}$ .
- (G) The HC-Gal4 expressing cell is not activated by a cold stimulus ( $\sim \Delta t = 5^\circ\text{C}$ ).



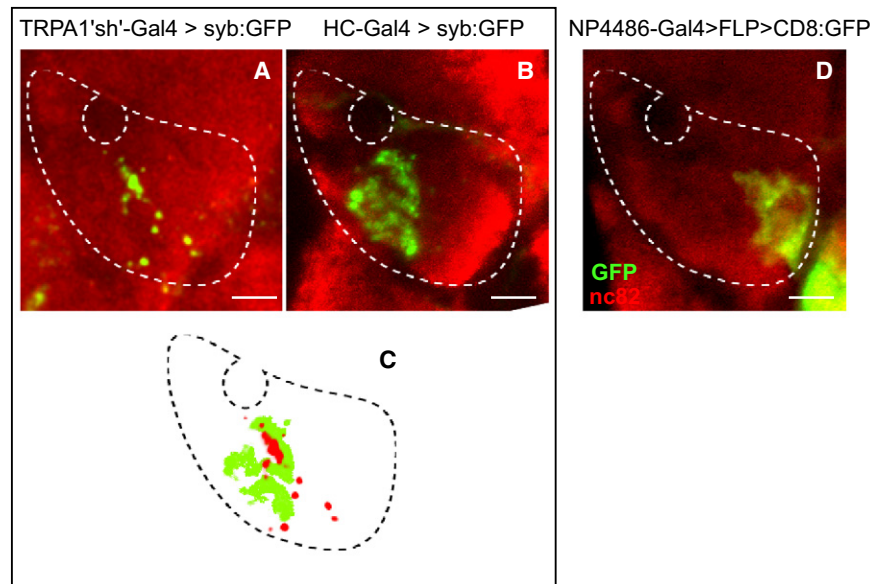


#### Figure S4. Convergence of Hot Fibers in the PAP, Related to Figure 4

An additional population of hot sensing cells has been recently described as an internal thermoreceptor (Hamada et al., 2008). Therefore, we examined if these candidate internal thermoreceptors might also send projections to the hot glomerulus.

(A) TRPA1<sup>'sh'</sup>-Gal4 (Hamada et al., 2008) in combination with UAS-syb:GFP reveals pre-synaptic processes deriving from “hot” internal thermoreceptors in the medial-anterior region of the PAP.

(B) Pre-synaptic processes from hot antennal receptors also target the medial-anterior region of the PAP (HC-Gal4 > UAS-syb:GFP).

(C) Graphic representation of the potential overlap between the two sets of projections (TRPA1<sup>'sh'</sup>-Gal4 projections are depicted in red and HC-Gal4 in green).

(D) Unlike hot projections, the afferents of antennal cold receptors arborize in the posterior region of the PAP. In all panels, presynaptic densities (syb:GFP in a,b) or afferent arborizations (CD8:GFP in e) are stained by anti-GFP; PAP landmarks are highlighted by staining with the unspecific synaptic marker nc82, in red (scale bar 50 μm).

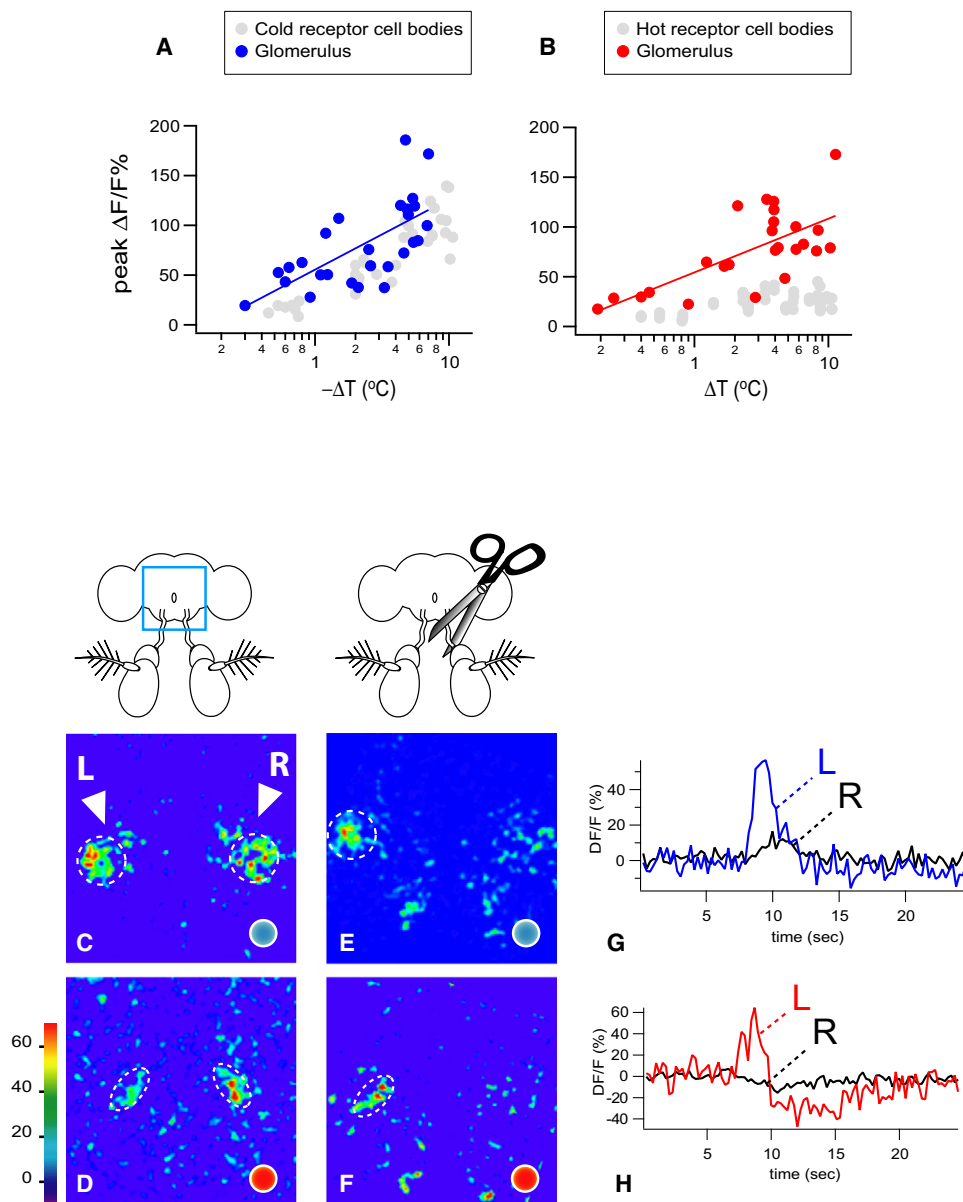


**Figure S5. PAP Responses to Temperature Stimuli Are Similar to the Antennal Ones and Depend on the Antenna, Related to Figure 5**

#### Antennal and Glomerular responses to temperature stimuli

(A and B) Stimulus-response plots for antennal cold and hot receptors recorded at the cell bodies (gray dots) and at the level of the corresponding PAP glomeruli (blue and red dots). Data from Figure 3, Figure 5, and Figure S3 are combined here and re-plotted on a logarithmic scale to resolve the responses to very small temperature stimuli, and to facilitate comparison between datasets. Calcium responses of (A) cold and (B) hot glomeruli (blue and red dots, respectively) are exquisitely sensitive, starting at small temperature changes ( $0.2\text{--}0.3^{\circ}\text{C}$ ). Notably, the response properties of hot and cold glomeruli are very similar, despite the differences observed at the cell bodies of the corresponding receptors (gray dots in a and b represent receptor responses).

#### Antennal thermoreceptors are major drivers of temperature activity in the PAP

Uni-lateral de-afferentiation reveals the contribution of antennal thermoreceptors to the activity of the PAP. (C–F) Low-magnification, two-photon imaging responses of a preparation expressing G-CaMP pan-neuronally (under *elav-Gal4*), responding to hot and cold stimulation ( $\Delta t \sim 5^{\circ}\text{C}$ ). Symmetrical responses to (C) cold and (D) hot stimuli are evident when both antennal nerves are intact (in c “L” denotes the left side of the brain; in c-f a blue spot represents a cold stimulus; red spot: hot stimulus). (E and F) Surgical resection of a single antennal nerve nearly abolishes temperature responses on the side of the lesion with little effect on the contralateral side. (G and H)  $\Delta F/F\%$  traces of (G) cold glomeruli and (H) hot glomeruli in e and f, respectively (L: left glomerulus, R: right glomerulus. ROIs chosen to calculate  $\Delta F/F$  values were of the same size and approximate position as the dashed circles in [C]–[F]).